Appendix S1
Supporting Information for
Size-based ecological interactions drive food web responses to climate warming

Max Lindmark[a,1], Jan Ohlberger[b], Magnus Huss[c], Anna Gårdmark[c]

[a] Swedish University of Agricultural Sciences, Department of Aquatic Resources, Institute of Coastal Research, Skolgatan 6, Öregrund 742 42, Sweden

[b] School of Aquatic and Fishery Sciences (SAFS), University of Washington, Box 355020, Seattle, WA 98195-5020, USA

[c] Swedish University of Agricultural Sciences, Department of Aquatic Resources, Skolgatan 6, SE-742 42 Öregrund, Sweden

[1] Author to whom correspondence should be addressed. Current address:
Max Lindmark, Swedish University of Agricultural Sciences, Department of Aquatic Resources, Institute of Coastal Research, Skolgatan 6, Öregrund 742 42, Sweden, Tel.: +46(0)104784137, email: max.lindmark@slu.se

Contents

1. Functions in the empirical stage structured biomass model

Table S1 Model functions. Note that dependencies are only expressed for state variables, but all functions relate to individual-level or mass-specific rates that depend both on body size and temperature.

Function	Expression	Description
Temperature		
$\boldsymbol{r_Y(T)}$	$e^{\frac{E_Y(T-T_0)}{kTT_0}}$	Function scaling rate/parameter Y with temperature ($Y = M, I_{max}, a, \mu, R_{max}, \delta$)
Consumer		
$\boldsymbol{\eta_{J,A}(R)}$	$a_{J,A}R$	Encounter rate
$\boldsymbol{I_{J,A}(R)}$	$\frac{\eta_{J,A}(R)}{1+\frac{\eta_{J,A}(R)}{I_{max,J,A}}}$	Ingestion rate
$\boldsymbol{v_{J,A}(R)}$	$\sigma_z I_{J,A}(R) - M_{J,A}$	Net-biomass production
$\boldsymbol{v^+_{J,A}(R)}$	$v_{J,A}(R)\ if\ v_{J,A}(R) > 0;$ $0\ otherwise$	Net-biomass production limited to positive values
$\boldsymbol{\gamma(v_J^+, \mu_J)}$	$\frac{v_J^+(R) - \mu_J(P)}{1 - z^{1-\frac{\mu_J(P)}{v_J^+(R)}}}$	Juvenile maturation rate
$\boldsymbol{\mu_J(P)}$	$r_\mu \varphi_1 {m_J}^{\varphi_2} + \frac{I_{PJ}(J,A)}{J}P$	Total juvenile mortality
$\boldsymbol{\mu_A(P)}$	$r_\mu \varphi_1 {m_A}^{\varphi_2} + \frac{I_{PA}(J,A)}{A}P$	Total adult mortality
Predator		
$\boldsymbol{\eta_{PJ}(J)}$	$pa_P J$	Encounter rate on juveniles
$\boldsymbol{\eta_{PA}(A)}$	$(1-p)a_P A$	Encounter rate on adults
$\boldsymbol{I_{PJ}(J,A)}$	$\frac{\eta_{PJ}(J)}{1+\frac{\eta_{PJ}(J)+\eta_{PA}(A)}{I_{max,P}}}$	Ingestion rate on juveniles
$\boldsymbol{I_{PA}(J,A)}$	$\frac{\eta_{PA}(A)}{1+\frac{\eta_{PJ}(J)+\eta_{PA}(A)}{I_{max,P}}}$	Ingestion rate on adults
$\boldsymbol{v_P(J,A)}$	$\sigma_p[I_{PJ}(J,A) + I_{PA}(J,A)] - M_P$	Net-biomass production
$\boldsymbol{\mu_P}$	$r_\mu \varphi_1 {m_P}^{\varphi_2}$	Background mortality

2. Parameterization of the empirical stage-structured biomass model

2.1 Body sizes

The core consumer-resource model was parameterized in (Lindmark *et al.* 2018). Here we add a predator feeding on the consumer to study a tri-trophic food chain. The state variables, i.e. species, and

for the consumer population (here represented by the freshwater zooplanktivorous fish roach, (*Rutilus rutilus*, L.) also the different life stages, are characterized by their representative body sizes. The representative weight of juvenile consumers (m_J) is derived using the equation: $m_J = \frac{m_{max}-m_{min}}{\ln(m_{\max})-\ln(m_{min})}$, where m_{min} is the weight of consumers at the onset of active feeding and m_{max} is the weight at maturation, following the approach in (van Leeuwen *et al.* 2008). m_{min} was acquired by converting length at onset of active feeding (approximately 10 mm) (Byström & García-Berthou 1999), to mass using the weight-length relationship presented in (Froese *et al.* 2014) ($\lambda_{C1} = 0.00794$ (constant) and $\lambda_{C2} = 3.15$ (exponent)). This resulted in $m_{min} = 0.0079$ g. With a length at maturation equalling 140 mm (Stoessel 2014), m_{max} becomes 32.4 g. The representative size of juveniles, m_J, then becomes 3.9 g. As we assume that adults use all their energy for reproduction and therefore do not grow in size, $m_A = m_{max} = 32.4$ g. The newborn (onset of active feeding in this case, 0.0079 g) to adult body size ratio (z), which is used in the maturation function (γ) (De Roos *et al.* 2008), is given by $m_{min}/m_{\max}$. This yields a value of $z = 0.00025$ (Table S2), which is in line with previous studies (van de Wolfshaar *et al.* 2012).

The predator, here based on northern pike (*Esox lucius*, L.), is not stage-structured and is therefore represented by a single body size. This is because we want to focus the analysis on the feedbacks between predator performance and predation-induced changes in prey (consumer) stage structure, which has been shown in empirical systems, e.g. (Persson *et al.* 2007), and how temperature-effects on the food chain depend on these feedbacks. We choose the value for the representative body size of the predator (642.6 g) to ensure equal attack rates of the predator on both consumer life stages (attack rate is a function of the length of both the attacker and the victim – see Fig. S1). This was done to separate the effects of predator body size (and thus varying attack rates) from the predator feeding intensity on the different consumer life stages, which we control with parameter p (Table S2). See section 2.2.2 below for more detailed information.

97 *Table S2 Parameter values at 19 °C. See text for references and specific parameters in allometric functions.*

Parameter	Value					Unit	Description	Reference
$\boldsymbol{k}$	8.617332e-05					eV K^{-1}	Boltzmann's constant	
$\boldsymbol{z}$	0.00025					-	New born to adult body size ratio (consumer)	(Byström & García-Berthou 1999; Stoessel 2014; Lindmark *et al.* 2018)
$\boldsymbol{\delta}$	0.1					day^{-1}	Turnover rate of shared and adult resource	(De Roos & Persson 2001, 2013; van de Wolfshaar *et al.* 2006) (see Box 3.4 in De Roos & Persson (2013))
$\boldsymbol{R_{max}}$	varied (0-2.6;1.7 default)					$g\ m^{-3}$	Maximum resource biomass density	See text above
$\boldsymbol{p}$	varied (0-1)					-	Predator foraging preference for juvenile consumers	
$\boldsymbol{\sigma_{z,p}}$	0.3 (zooplanktivory, consumer) 0.4 (piscivory, predator)					-	Assimilation efficiency	(van Leeuwen *et al.* 2008)
$\boldsymbol{E_Y}$	E_M	E_I	E_μ	$E_{R_{max}}$	E_δ			
	0.594	0.594*	0.45	varied (-0.43, 0)	0.43	eV	Activation energy of metabolism, functional response parameters, mortality, maximum resource density (with/without) and resource turnover rate	(Savage *et al.* 2004; Ohlberger *et al.* 2011, 2012; Lindmark *et al.* 2018)
	Juvenile Consumer (J)		Adult Consumer (A)		Predator (P)			
$\boldsymbol{m_{J,A,P}}$	3.9		32.4		642.6	g	Representative body size	(Lindmark *et al.* 2018)
$\boldsymbol{M_{J,A,P}}$	0.009		0.006		0.004	$g\ g^{-1}\ day^{-1}$	Metabolic rate**	(Diana 1982; Ohlberger *et al.* 2012), see text
$\boldsymbol{I_{max,J,A,P}}$	0.183		0.112		0.057	$g\ g^{-1}\ day^{-1}$	Maximum ingestion rate**	(Hölker 2000), see text
$\boldsymbol{a_{J,A,P}}$	25.972		9.083		0.018	$m^3\ g^{-1}\ day^{-1}$	Attack rate	(Claessen *et al.* 2000; Hjelm & Persson 2001; De Roos & Persson 2013) (see Fig. 11.2 in De Roos & Persson (2013))
$\boldsymbol{\mu_{J,A,P}}$	0.001		0.0006		0.0003	day^{-1}	Background mortality	(De Roos & Persson 2013)

* This parameter is also varied between 0.297 and 0.891 in Fig. S11-S12 and Table S6

** Note that metabolic rate and/or maximum ingestion rate also change with temperature differently for different sizes when $c_{M,I} \neq 0$ (see section 2.2.4 and Eq. S1)

2.2 Mass- and temperature dependence of individual-level rates

We model the following vital rates and parameters as temperature dependent: metabolism ($M_{J,A,P}$), the functional response via the parameters maximum ingestion rate ($I_{max,J,A,P}$) and attack rate ($a_{J,A,P}$), as well as background mortality ($\mu_{J,A,P}$) of the consumer and the predator, and turnover rate (δ) and maximum density (R_{max}) of the basal resource. Subscripts J, A, P refer to juvenile consumers, adult consumers and predators, respectively, which are characterized by their body size (Table S1-S2). Temperature dependence is acquired using an Arrhenius term $r_Y = e^{\frac{E_Y(T-T_0)}{kTT_0}}$, where T [K] is the temperature, T_0 [K] is an arbitrary reference temperature (here 292 $^\circ$ K), k [eV K^{-1}] is Boltzmann's constant and E_Y [eV] is the activation energy of rate or parameter Y (Gillooly *et al.* 2001) – see main text and Table S2. Below follows a more detailed description and derivation of the size- and temperature-dependent functions $M_{J,A,P}$, $\sigma_{J,A,P}$, $I_{max,J,A,P}$ and $\mu_{J,A,P}$.

2.2.1 Metabolism

Importantly, for metabolism we also allow temperature to affect the size dependence of the metabolic rate through parameter c, which scales the allometric exponent of metabolism (ρ_2' at the reference temperature) linearly with temperature (in accordance with empirical studies, (Ohlberger *et al.* 2012; Lindmark *et al.* 2018)). Only the numerical values of the temperature-dependent allometric functions at 19 °C are presented in Table S2 for clarity – but note that when $c \neq 0$, the metabolism is not only scaled by the r_M-function but also with a temperature-effect on the size dependence (allometric exponent). The temperature- and size-dependent metabolism is modelled as

$$M_{J,A,P} = r_M \rho_1 m_{J,A,P}^{\rho_2' + c(T-T_0)} \quad \text{(S1)}$$

where ρ_1 is the allometric constant (see below), ρ_2' is the allometric exponent at 19 °C and c is a linear temperature dependence of the allometric exponent (see section 2.2.4) We varied the c-parameter in the main analysis to study the effect of temperature-independent size-scaling of metabolism ($c = 0$) as well as the case when warming increases metabolic rate more for large individuals than small ones (i.e., $c > 0$, here $c = 0.005$). For the consumer population, the parameters ρ_1, ρ_2' and E_M are derived from experiments on roach (van de Wolfshaar *et al.* 2006; Ohlberger *et al.* 2012). E_M is 0.594 [eV], similar to values found in other studies (Downs *et al.* 2008), and $\rho_2' = 0.77$ (van de Wolfshaar *et al.* 2006). We rescaled the allometric constant (ρ_1) to unit g wet weight, assuming an energy density of 6000 J g^{-1}, in line with previous studies (Pothoven *et al.* 2006; Lumb *et al.* 2007; van Leeuwen *et al.* 2008; van de

Wolfshaar *et al.* 2012) and to a new reference temperature (19 °C, instead of 0 °C). This resulted in a value for ρ_1 of 0.0123 $g^{(1-\rho_2')}$ day^{-1} (Lindmark *et al.* 2018).

In this study, we assumed equal temperature dependence (activation energy) for the predator species as for our consumer species (i.e. the same r_M), but derived species-specific allometric parameters for the predator's metabolic rate based on experiments on pike (Armstrong *et al.* 1992). In (Armstrong *et al.* 1992), the allometric function describing resting metabolic rate (oxygen consumption) at 15 °C was estimated to be $V_{O_2} = 0.162 m_P^{0.8}$ [mg O_2 h^{-1}]. Using the relationship $1\,\text{kcal}\,\text{kg}^{-1}\,\text{h}^{-1} = 308\,\text{mg}\,O_2\,\text{kg}^{-1}\,\text{h}^{-1}$ (Groot 2010), we rescaled the metabolic rate for a representative predator weighing 642.6 g to unit g g^{-1} day^{-1}. Assuming 1 cal = 4.1855 J at that temperature, metabolic energy demand is 2226 cal day^{-1}, or 9316 J day^{-1}. With an energy density of 3600 J g^{-1} for pike (Heikinheimo & Korhonen 1996), the mass-specific metabolic rate becomes 0.004 g g^{-1} day^{-1} at 15 °C. The parameter ρ_1 in the equation for metabolism (Eq. S1) then becomes 0.0147 $g^{(1-\rho_2')}day^{-1}$ for pike at 15 °C, using the same conversions. This can be rescaled to our reference temperature (19 °C) by dividing it with 0.7207 ($M_{P,15^\circ\text{C}}/M_{P,19^\circ\text{C}}$, given the constant ρ_1 at 15 °C), yielding a ρ_1 of 0.02 [$g^{(1-\rho_2')}$ day^{-1}] at 19 °C. Lastly, Diana (1982) shows that the allometric exponent (ρ_2') for pike is strongly dependent on temperature, but only two temperatures are given in that study. We therefore approximated a value at 19 °C by assuming a linear temperature effect on the exponents ($\rho'_{2,2^\circ\text{C}} = 0.97$ and $\rho'_{2,14^\circ\text{C}} = 0.82$), resulting in $\rho'_{2,19^\circ\text{C}} = 0.76$. With these parameters, the mass-specific metabolic rate at 19 °C is 0.0043 g g^{-1} day^{-1} for the predator, using Eq. S1. The resulting mass-specific metabolic rates are close to previous studies using similar models with other piscivorous fish (van Leeuwen *et al.* 2008; van Denderen & van Kooten 2013). However, it should be noted that the variation in metabolic rate for pike is very large in the literature – even when accounting for the effects of size and temperature (Armstrong & Hawkins 2008). Because metabolism is the major loss term in the biomass dynamics of the predator, the exact value in relation to their ingested energy will shape their biomass densities at equilibrium for a given $R_{max,T19}$, and therefore their ability to persist in warmer environments (see section 2.2.3 below for parameterization of the resource). Thus, when making quantitative predictions, accurate descriptions of both the bio-energetics and habitat $R_{max,T19}$ are key parameters, as well as the feeding preference of the predator. In this study, we focus on exploring the range of qualitative dynamics to identify the mechanisms driving potential changes in community dynamics and structure.

2.2.2 Feeding rate

Ingested energy, $I_{J,A}(R)$, $I_{PJ}(J,A)$ and $I_{PA}(J,A)$ for consumer life stages and the predator species, respectively, follows a Holling type II functional response (Holling 1959) (Table S1), with size- and temperature-dependent functions describing maximum ingestion ($I_{max,J,A,P}$) and attack rate ($a_{J,A,P}$). $I_{max,J,A,P}$ is an allometric function given by $r_I \varepsilon_1 m_i^{\varepsilon_2 + c_I(T-T_0)}$. We estimated parameters ε_1, ε_2, c_I and

the activation energy, E_I within the temperature scaling function $r_I = e^{\frac{E_I(T-T_0)}{kTT_0}}$, from data on estimated allometric functions at different temperatures, provided in (Hölker 2000) (Table S3).

Table S3. Results from the nls model used to estimate parameters in allometric functions for $I_{max,J,A}$

Parameter	Estimate	Standard error	t-value	Unit
$\boldsymbol{\varepsilon_1}$	0.248	0.004	61.97	$g^{(1-\varepsilon_2)}day^{-1}$
$\boldsymbol{\varepsilon_2}$	0.767	0.003	234.28	-
$\boldsymbol{E_I}$	1.206	0.032	37.27	eV
$\boldsymbol{c_I}$	-0.011	0.001	-12.32	$°C^{-1}$

These data stem from ad-libitum feeding experiments of roach weighing 1.2-300 g performed at temperatures between 5 °C and 20 °C (presented in unit g day^{-1}). Non-linear least-squares regression (*nls* function in R version 3.4.2 (R Core Team 2018), using the Gauss-Newton algorithm) was used to estimate the parameters. We assumed identical scaling of $I_{max,J,A,P}$ for both predators and consumers. This is commonly done in physiologically structured population models (Claessen *et al.* 2000), and there is no clear biological reason for why the size dependence of handling time (or maximum intake rate as in our case) should differ significantly between prey types when the mode of feeding (active) is the same. The allometric constant may, however, be species-specific, but as we are not aiming to make quantitative predictions for a given species we believe this is an accurate approximation from a detailed and rare set of experiments with a fully-factorial design, a large size range, and multiple temperature replicates (Hölker 2000; Hölker & Haertel 2004). Note also that while intraspecific temperature dependence of $I_{max,J,A,P}$ (or handling time) shows remarkable variation (Dell *et al.* 2011a; Englund *et al.* 2011a), our estimate ($E_I = 1.206$ eV) is at the higher end of the range (0-1.2 eV) given in (Dell *et al.* 2011a). Therefore, in the default parameterization of the empirical model, we applied a value identical to the activation energy for metabolism ($E_I = E_M = 0.594$ eV), while keeping the other parameters as in Table S2. However, we also varied the temperature dependence of functional response parameters by scaling them relative to E_M using a factor of 0.5-1.5 (Table S2). These results are presented in sections 4.4.6 and. In section 4.4.7 we performed a similar analysis but also controlling for the temperature dependence of mortality.

We derive attack rates ($a_{J,A,P}$) for each consumer life stage and the predator. Note that even though the predator attack rates depend on the size of the consumer as well as the predator (Persson *et al.* 1998; Claessen *et al.* 2000; Hjelm & Persson 2001), in our model we choose a predator size that yields identical attack rates given the attack rate function and parameters used (see below) (Fig. S1), to separate the effects of size-dependent attack rate from predator feeding preferences (p, see above).

Consumer attack rate on zooplankton is modelled as $a_{J,A} = r_I \hat{A}\left[\frac{m_{J,A}}{o_z} exp\left(1 - \frac{m_{J,A}}{o_z}\right)\right]^{\alpha}$, where Â is the maximum attack rate (300 m^3 day^{-1}), o_z is the optimal forager size (41 g) and α is the size-scaling exponent (0.75). These attack rate parameters were estimated for roach from experiments with 1 mm *Daphnia* as prey (Hjelm & Persson 2001).

For the predator's attack rate on the consumer life stages, we follow the approach in Claessen et al (Claessen *et al.* 2000). This is a length-based approach in which the predation window (W) is the range of predator to prey (henceforth consumer) body length ratios that yield a positive attack rate. We used the weight-length relationships presented in (Froese *et al.* 2014) ($\lambda_{P1} = 0.00447$ (constant) and $\lambda_{P2} = 3.08$ (exponent)) to convert length to mass for pike. The predation window, $W(l_P, l_{J,A})$, as a function of predator (l_P) and consumer ($l_{J,A}$) length (given by λ_{C1} and λ_{C2} – see section 2.1, is given by the following equation:

$$W(l_P, l_{J,A}) = \begin{cases} \frac{l_{J,A} - \vartheta_{min} l_P}{(\vartheta_{opt} - \vartheta_{min}) l_P} & if \quad \vartheta_{min} l_P < l_{J,A} \leq \vartheta_{opt} l_P \\ \frac{\vartheta_{max} l_P - l_{J,A}}{(\vartheta_{max} - \vartheta_{opt}) l_P} & if \quad \vartheta_{opt} l_P < l_{J,A} < \vartheta_{max} l_p, \\ 0 & otherwise \end{cases}$$

where ϑ_{min} is the minimum predator-consumer length ratio, ϑ_{opt} is the optimum length ratio and ϑ_{max} is the maximum predator-consumer length ratio for which predation is possible. We use the parameter values $\vartheta_{min} = 0.03$ and $\vartheta_{max} = 0.55$ for pike (Persson *et al.* 2006). As we could not find an estimate for ϑ_{opt} for pike, we adopted the default value of 0.2, based on the piscivorous predator perch (*Perca fluviatilis*, L.) presented in Claessen et al (Claessen *et al.* 2000). The relative attack rate that the predation window represents is multiplied with an allometric function of the form $\beta_1 l_p^{\beta_2} W(l_P, l_{J,A})$ to get absolute values in m^3 day^{-1}. We use the values $\beta_1 = 0.4$ and $\beta_2 = 0.6$ (Claessen *et al.* 2000; De Roos & Persson 2013) (see Fig. 11.2 in (De Roos & Persson 2013)). The representative body size of the predator was set to acquire the same attack rate by the predator on both consumer life stages, i.e. based on where the two attack-rate windows intersect for the two consumer life stages (Fig. S1), to disentangle the effect of predator feeding preference which we scale with parameter p, from those of its size-dependent attack rate.

The net energy gain is scaled by an assimilation efficiency, $\sigma_{p,z}$. We followed the approach in (van Leeuwen *et al.* 2008) and used the values 0.4 and 0.3 for piscivory (σ_p) and zooplanktivory (σ_z), respectively, and assumed assimilation efficiency to be temperature-independent (Peters 1983; Gilbert *et al.* 2014).

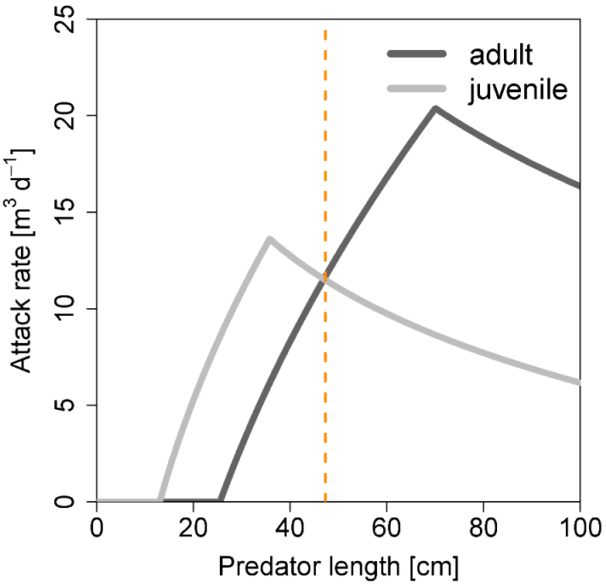

Fig. S1. Predator attack rate as a function of predator body length shown for adult (black) and juvenile (grey) consumers. Orange dashed line shows the predator length that gives equal attack rates on both consumer life stages, which is used to set the representative body size of the predator (47 cm, 642.6 g). See section 2.2 for equations.

2.2.3 Mortality

As in (Lindmark *et al.* 2018), we assumed a temperature-dependent allometric function for whole-organism background mortality of the form $r_\mu \varphi_1 m_{J,A,P}{}^{\varphi_2}$, where $\varphi_1 = 0.0015$ (De Roos & Persson 2013) (see Box 3.4 in (De Roos & Persson 2013)) and $\varphi_2 = -0.25$ (Gillooly *et al.* 2001) and E_μ within r_μ is set to 0.45 eV (Savage *et al.* 2004).

2.2.4 Temperature-size interactions

Note that while the temperature-size interaction term for maximum ingestion (c_I) is significantly different from 0 in the statistical model (Table S3), we only model temperature-effects on the metabolic exponents in the dynamical models for clarity and refer to that parameter as c (see also (Lindmark *et al.* 2018); Equation S1). It does not matter qualitatively which exponents are varied (positive effect on metabolism exponent or negative effect on maximum ingestion exponent), as both lead to steeper size-scaling of the critical resource density needed to meet basal metabolic demands (R_{crit}) in warmer environments (see main text). R_{crit} is given by $R_{crit} = \frac{M}{a(\sigma - \frac{M}{I_{max}})}$, where M is metabolic rate, σ is the assimilation efficiency, a is attack rate and I_{max} is maximum ingestion rate (Byström & Andersson 2005). For example, all else being equal, $c = 0.02$ leads to an 85.6% increase in R_{crit} for a 32.4 g individual (representative size for adult an consumer) at 26 °C relative to 19 °C (not shown), while $c_I = -0.01$ (i.e. interactive effect of size and temperature for maximum ingestion rate, as found in our

species) leads to a 5.7% increase over the same temperature range and for the same body size. Previous studies have found c to vary roughly between -0.02 and 0.02 (Ohlberger *et al.* 2012; Lindmark *et al.* 2018) for metabolic rate. If assuming a temperature-independent exponent of feeding rates (i.e. $c_I = 0$), $c = 0.02$ would lead to potentially large effects of temperature on the size-scaling of CRD. In this study we used a value of $c = 0.005$ (Fig. S2), which is lower than the upper range of c-values found in previous studies on intraspecific temperature effects (e.g. $c = 0.02$) (Ohlberger *et al.* 2012; Lindmark *et al.* 2018) (see also (Lindmark *et al.* 2018) for an assessment of the effect of c for a larger range of values, including negative values). With $c = 0.005$, R_{crit} increases by 15.9% for a 32.4 g individual. This is larger than the empirical estimate of our model species (see above). However, since it is substantially lower relative to potential effects of c on R_{crit} (when considering the empirical range found in a number of species (Ohlberger *et al.* 2012; Lindmark *et al.* 2018)), we view $c = 0.005$ as a small to moderate temperature-size interaction effect in terms of the effects on the size-scaling of R_{crit} at different temperatures.

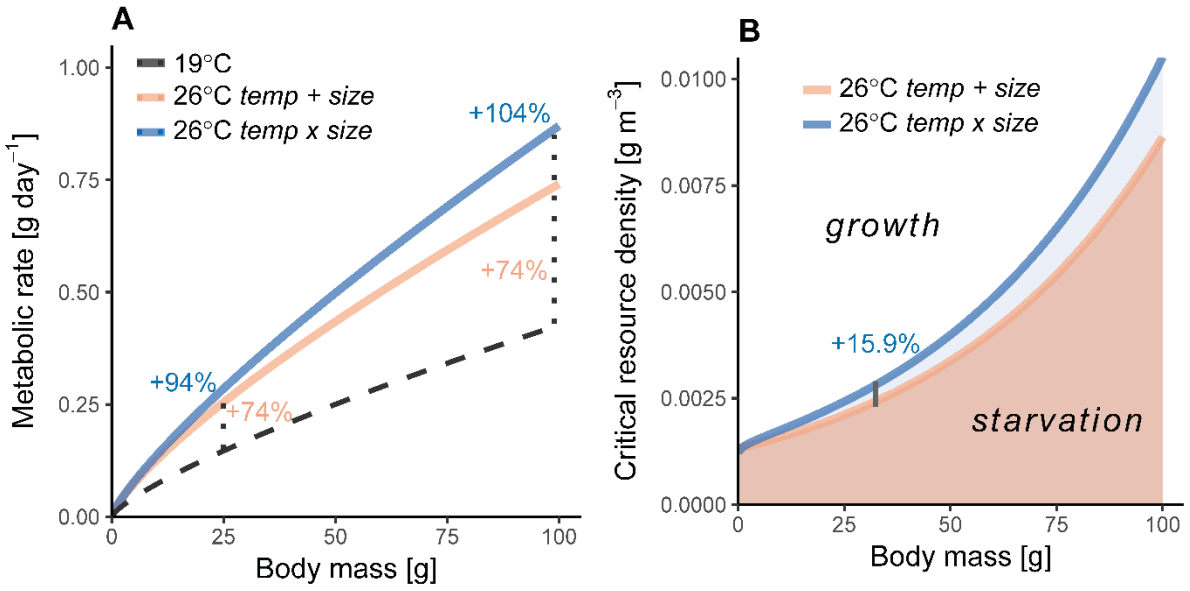

Fig. S2. Temperature- and size dependence of metabolic rate and the critical resource density (R_{crit}) needed to meet metabolic demands. Metabolic rate (A) and critical resource density (B) as functions of body mass for the consumer at 26 °C given positive interactive ($c = 0.005$) (blue) and independent ($c = 0$) (coral) effects of temperature and body size on metabolic rate. Black vertical dotted lines in panel (A) show 25 g and 99 g individuals for illustration purposes, for which metabolic rate is 94% and 104% higher at 26 °C relative to 19 °C when metabolism scales with a positive temperature-size interaction. In the case of independent temperature-size scaling, metabolism increases with 74% relative to 19 °C regardless of body mass. In (B) the effect of c is illustrated for a body size that represents the adult life stage in our study species (vertical line), for which the critical resource density increases by 16% when $c = 0.005$ compared to when $c = 0$.

2.3 Resource

We used the activation energy of resource turnover rate ($E_\delta = 0.43$) as in (Lindmark *et al.* 2018) which was acquired by fitting a non-linear least-squares regression to the increasing part of the hump-shaped temperature dependence used in (Ohlberger *et al.* 2011) (s.e. = 0.01098, t = 39.42, p < 0.0001). This hump-shaped curve stems from a bioenergetics model (Karås & Thoresson 1992), where parameters for optimum- and maximum growth temperatures are derived from within-species population growth data (Mitchell *et al.* 2004) (Fig. S3).

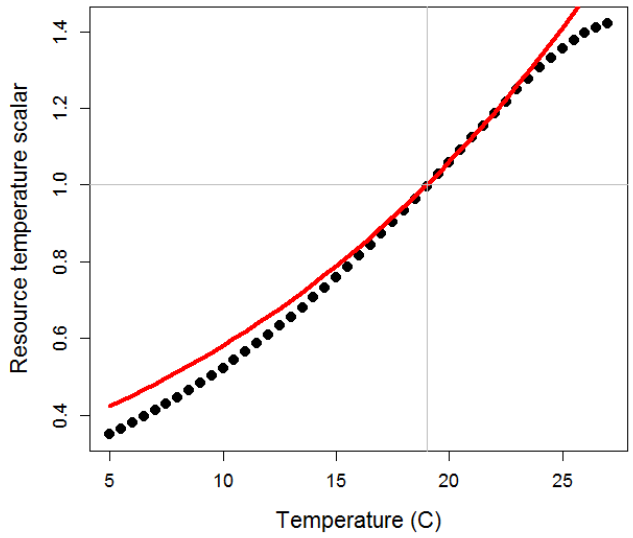

Fig. S3. Simulated resource temperature scalar from Ohlberger *et al.*, (2011) based on the bioenergetics model in Karås & Thoresson (1992) and data from Mitchell *et al.*, (2004) (black points). The red line is the fit of the nls model to these simulated data, yielding an activation energy of $E_\delta = 0.43$. This is the default value used in the main analysis (which also applies to $E_{R_{max}}$, see main text), but it also varied in Table S5-S6.

To capture a broad range of realistic temperature dependencies of resource growth, we varied the temperature dependence of $R_{max,T19}$ (19 °C) with parameter $E_{R_{max}}$ (Fig. 2). We did this by assuming two contrasting scenarios; no effect of temperature on $R_{\text{max,T19}}$ ($E_{R_{max}} = 0$) or $R_{\text{max,T19}}$ declining with the same rate as turnover rate increases (i.e. $E_{R_{max}} = -E_\delta = -0.43$ [eV]), based on mass conservation and metabolic scaling principles (Gilbert *et al.* 2014) – see also methods section in the main text. The resource turnover rate at reference temperature (19 °C) was assumed to be 0.1 (De Roos & Persson 2001, 2013; van de Wolfshaar *et al.* 2006). $R_{\text{max,T19}}$ was varied between 0 and 2.6 [g m^{-3}] in the analysis. This range was chosen to ensure both persistence of predators and non-cyclic dynamics in most of the parameter space. Note that with increasing $R_{\text{max,T19}}$, the parameter regions with cyclic dynamics increase (Fig. S8).

3. Regulation of the consumer population

In stage-structured biomass models with two life stages (adults and juveniles), competitive asymmetry between juveniles and adults ("*ontogenetic asymmetry"*) refers to juveniles or adults being more limited by resources than the other. This implies that the life stage with the least efficient biomass production becomes an energetic bottleneck. Several studies have pointed out that the most important consequence of ontogenetic asymmetry is an overcompensatory response in biomass to mortality (De Roos *et al.* 2007; Persson & De Roos 2013). This is due to mortality relaxing resource competition, to which the most resource-limited stage responds with increased net biomass production, which can manifest itself in higher rates of per capita and population-level reproduction or maturation, depending on which stage is more resource limited. Ultimately, this leads to a hump-shaped relationship between biomass density at equilibrium and mortality (usually of one life stage).

As our main results of alternative stable states emerging in warmer environments, are due to the presence or absence of biomass overcompensation (induced by predation in this case), we here explain how the consumer population is regulated in terms of which life stage is the more efficient biomass producer and its consequences for the effect or mortality (Table S4). In the absence of predators, the consumer population is limited by slow reproduction and the adult life stage is an energetic bottleneck in terms of biomass production (Persson & De Roos 2013). This can be predicted by the lower critical resource density (R_{crit}) of juveniles (see Fig. S2B) when both life stages compete for a shared resource. Inspection of the rates of maturation and reproduction at equilibrium when the predator is extinct verifies that reproduction is lower than maturation at high temperatures (Fig. S4B and see also Table S4 for results at reference temperature without predators). This asymmetry in net biomass production (adult energetic bottleneck) in the consumer population is what causes the overcompensatory response to increased mortality when predators predominantly target juveniles (De Roos *et al.* 2007). To generalize our results on stability and persistence over temperature and link them to the stage-structure in the consumer population, we also redo the main analysis with the original (generic) parameterization (De Roos *et al.* 2007; De Roos & Persson 2013) of the model while also varying the regulation of the consumer population with the phenomenological parameter q, see section 5.

Table S4 Characteristics of the stage-structured consumer population in absence of predation mortality at reference temperature using the empirical model with default parameterization.

Characteristic	**Result in empirical model (default parameters) without predators**
Which life stage has the lowest critical resource density?	Juveniles, which indicate they are superior competitors for a shared resource (see Fig. S2B)

Which life stage is more dominant in terms of biomass density at equilibrium?	Adults (Adults=6.58 [g m^{-3}], Juveniles=1.04 [g m^{-3}])
Which rate is largest at equilibrium (maturation vs reproduction)?	Maturation, causing a pile-up of biomass in the adult life stage (maturation = 0.004 [g m^{-3} day^{-1}] reproduction = 1.51e-05 [g m^{-3} day^{-1}])
Is there overcompensatory response to mortality?	In Juveniles, as lower consumer biomass (from mortality) reduces competition which increases per capita and population level reproduction of adults, causing an increase in juvenile biomass density at equilibrium

3.1 In the presence of a predator

In the presence of a juvenile specialized predator (Fig. S4B), predation releases the adult consumer life stage from strong intraspecific competition, resulting in a larger reproductive output than when predators do not shape the stage structure of the consumer (Fig. S4A, or when predators are extinct in Fig. S4B high temperatures; Table S4 for reference temperature without predators). In the latter scenarios, a slow reproduction is the bottleneck of the consumer population. Therefore, a juvenile-specialized predator promotes its own food source by inducing a high reproductive output in its prey species. The general decline in predator biomass density with warming impacts the stage structure of the consumer population (Fig. S5), and this is more drastic in the case of a predator feeding predominantly on juveniles (Fig. S5B). Eventually the regulation of the consumer population also changes (when predators collapse). This is evident in that with predators present (low temperatures in Fig. S4B), consumer maturation rate is lower than the reproductive output, whereas when predators are extinct (high temperatures in Fig. S4B) a slow reproduction instead limits consumer population growth. When predators feed on both life stages they do not change the stage structure of the consumer to an extent that alters their regulation. This is the mechanism behind biomass overcompensation, which occurs when mortality releases the consumer life stage that limits population growth from high density dependence.

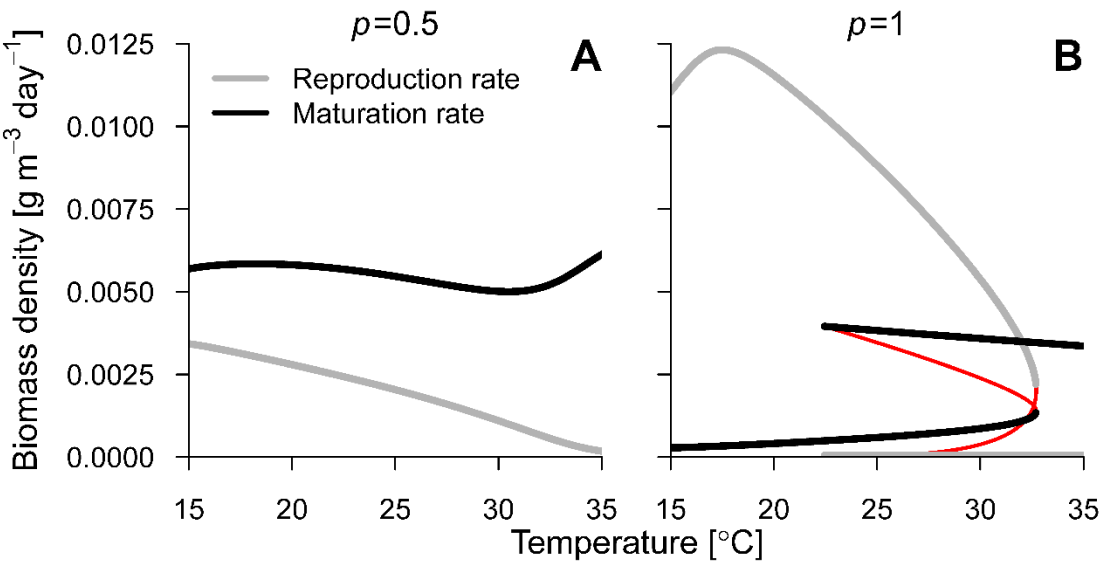

Fig. S4. Population-level maturation ($\gamma[v_J^+(R,P)]J$) (black) and reproduction ($v_A^+(R)A$) (grey) rate in the consumer population (see Table S1) at equilibrium as a function of temperature, for a predator feeding with equal intensity on both life stages (A) ($p = 0.5$) and a predator feeding exclusively on juveniles (B) ($p = 1$). When reproduction and maturation rates differ (in terms of biomass density per unit time), the growth of the consumer population is limited by the lower of the two rates. In this figure, the consumer life stage is limited by low reproductive output from adults, unless juvenile-specialized predators are present (B) at sufficiently high densities to induce a shift in the stage structure of the consumer such that it becomes dominated by juveniles, leading to a slow maturation rate relative to the reproductive output of adults. $E_{R_{max}} = -0.43$, all other parameters have default values.

3.2 Ratio of juvenile to adult biomass density

Fig. S5 illustrates the juvenile to adult biomass ratio at equilibrium in the empirical model. It shows that in the stable equilibrium with coexistence, the juvenile to adult biomass ratio decreases with temperature, and does so more rapidly with positive temperature-size interactions ($c = 0.005$). This is likely because temperature-size interactions induce a proportionally stronger negative effect on the energetic efficiency of adults, which reduces the reproductive output and thus juvenile biomass (but note the predator biomass density, which shapes the consumer stage structure through predation, is also affected by $c = 0.005$). Thus, persistence of a juvenile-specialized predator ($p = 1$; Fig. S5B) is reduced when $c = 0.005$ relative to $c = 0$.

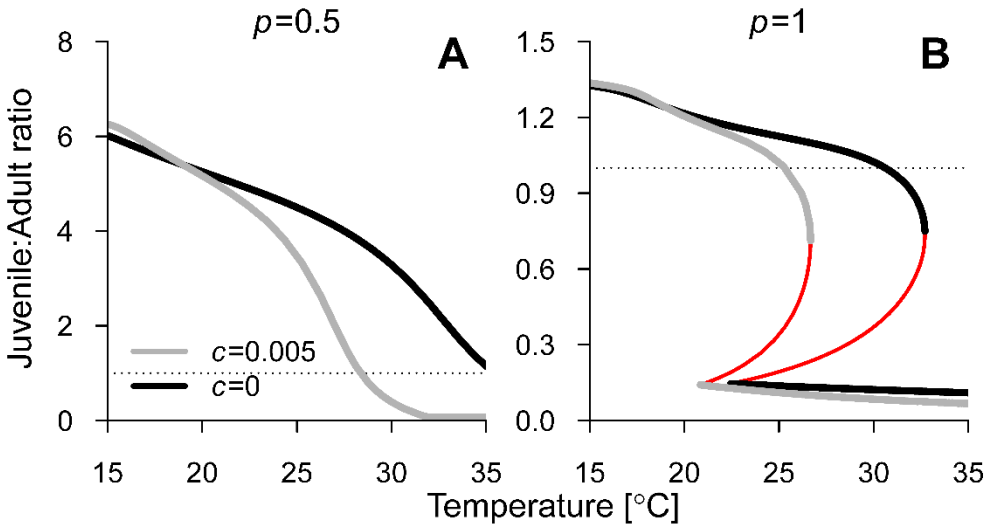

Fig. S5. Ratio of juvenile to adult biomass at equilibrium as a function of temperature for a predator feeding with equal intensity on both consumer life stages (A) ($p = 0.5$) and a predator feeding exclusively on juveniles (B) ($p = 1$), for two temperature-size scaling scenarios for the consumer and predator. $c = 0$ (black lines) refers to independent effects of size and temperature and $c = 0.005$ (grey lines) means interactive effects of temperature on the size-scaling exponent of metabolism. Horizontal dotted lines show 1:1 juvenile to adult biomass ratios. When predators feed exclusively on juveniles (panel B), bistability emerges (then unstable equilibria which connect the two stable equilibria are shown with thin red lines for completeness). The interactive temperature-size scaling for metabolism shifts the stage structure in the consumer population, by reducing the energetic performance of adults, leading to reduced reproductive output (see Fig. S4 and corresponding figure text for reproduction vs maturation rate and how these rates regulates the consumer population). Note the different scales on the y-axes and that in B, the consumer stage structure is no longer shaped by predation as predators are extinct. $E_{R_{max}} = -0.43$ and all other parameters have default values.

4. Parameter sensitivity of the empirical model

In this section, additional analyses to supplement the main analysis are presented. The results are described and explained in the corresponding sections and figure legends.

4.1 Maximum resource density shapes coexistence

As maximum resource density, $R_{max,T19}$, largely determines the community structure and composition for a given temperature, we first performed continuation analysis of equilibria over R_{max} at 19 °C (reference temperature, where all temperature scaling functions, r_Y, equal 1) (Fig. S6). This was done in order to find a default $R_{max,T19}$ (Table S2) that ensures coexistence without a dominance of cyclic

equilibrium dynamics, given default parameters (e.g. Fig. S8). Note, however, that we also vary the parameter $R_{max,T19}$ in the main analyses (Fig. 2, main text). From low to high $R_{max,T19}$-values, consumers can first invade a stable resource-only system. Then, depending on the type of feeding preference in the predator, predators can either persist (limit point, saddle node bifurcation) ($p = 1$) or invade (branching point, transcritical bifurcation) ($p = 0.5$). In the case of $p = 1$, invasion occurs at higher temperatures than temperatures allowing for persistence, which gives rise to bistability where predators are either absent or present. Above this $R_{max,T19}$-value (~1.3), all species can coexist. From this point, if predators feed equally on both life stages ($p = 0.5$), higher $R_{max,T19}$ results in cyclic dynamics (Hopf bifurcation)

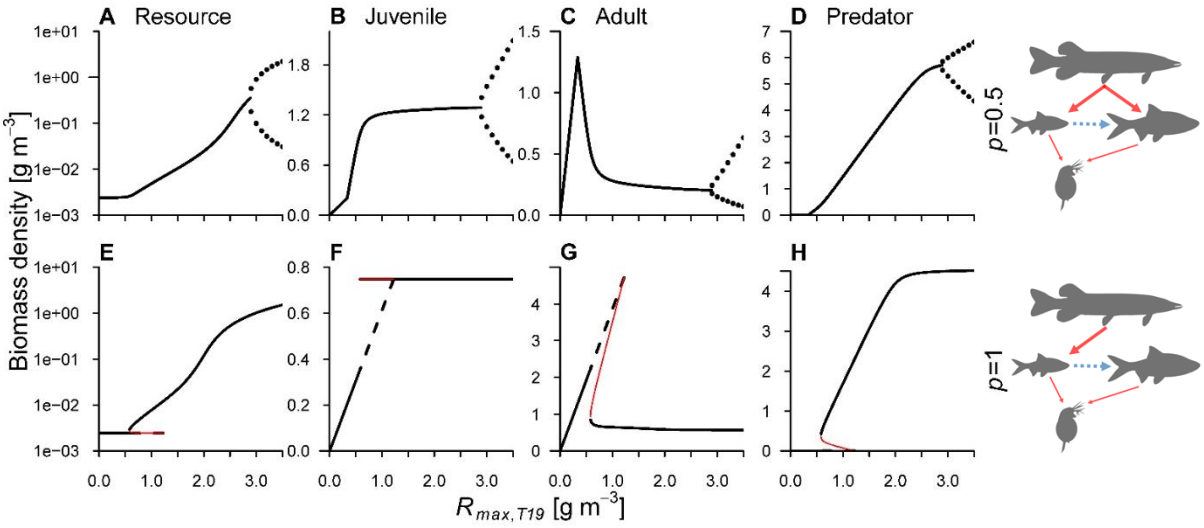

Fig. S6. Effects of $R_{max,T19}$ on food chain stability depend on ecological interactions. Equilibrium biomass densities of the resource (A, E), consumer life stages (B-C, F-G) and predator (D, H) as a function of $R_{max,T19}$, given a predator feeding with equal intensity on both life stages (A-D) ($p = 0.5$) or exclusively on juveniles (E-H) ($p = 1$). Black lines (full and dashed) are stable equilibria and red thin lines are unstable equilibria (connecting the two stable branches in the bistable region, shown for completeness), which separate the two stable equilibria when there are alternative stable states. Maximum and minimum biomass of a stable limit cycle is shown with points (top row, $R_{max,T19} >$ 2.9). Alternative stable states, where predators are either extinct or abundant, occur between $R_{max,T19}$ ~ (0.6-1.2) in E-H. Note the different scales on the y-axes and the logarithmic y-axis for resources densities. Temperature is 19 °C and all parameters have default values.

4.2 Equilibrium biomass densities over temperature for different $R_{max,T19}$ ($p = 1$)

Fig. S7 illustrates the change in equilibrium biomass densities over temperature for three selected $R_{max,T19}$-values, representing high, medium and low $R_{max,T19}$-values (covered in Fig. 2, main text), and no (upper panel) and negative (lower panel) effects of temperature on $R_{max,T19}$. Its main purpose is to complement Fig. 2 (main text) and to show actual biomass densities in addition to the bifurcation

points shown in Fig. 2. This shows at which biomass densities predators collapse because they are not able to control the stage-structure of their prey (Fig. S7H). It also shows that more productive (higher $R_{max,T19}$) systems lead to higher biomass densities of predators, which allows them to persist at higher temperatures. This is because biomass is transferred up in the food chain from the basal resource and is built up in the predator population (De Roos & Persson 2013), which also explains why the consumer biomass density at equilibrium does not change with $R_{max,T19}$ when predators are present (Fig. S7B-C, F-G).

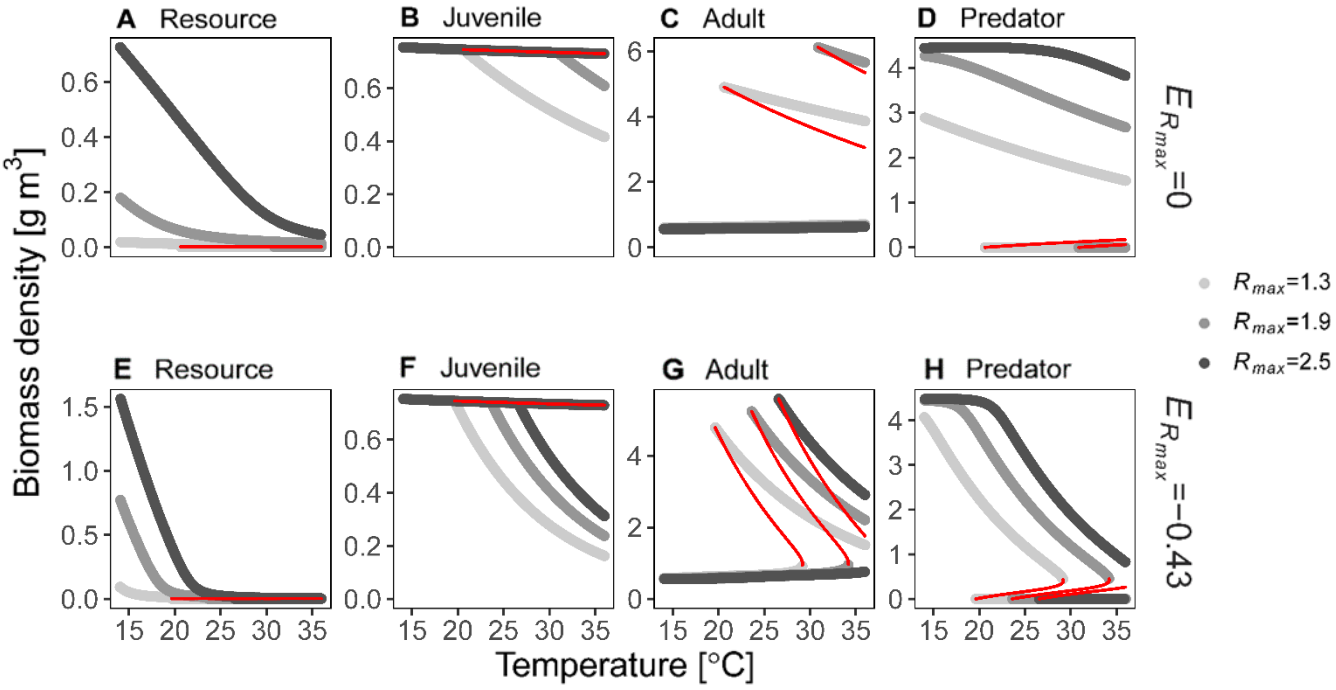

Fig. S7. Equilibrium biomass densities of the resource (A, E), juvenile (B, F) and adult (C, G) consumers and predator (D, H) as a function of temperature for three different levels of $R_{max,T19}$. The chosen $R_{max,T19}$ levels reflect the range of values used in Fig. 2 (main text) for the predator feeding exclusively on juveniles ($p = 1$). The top row shows biomass densities when assuming no effect of temperature on $R_{max,T19}$ and in the bottom row it is assumed that $R_{max,T19}$ decreases with temperature ($E_{R_{max}} = 0$ and -0.43, respectively). Thin red lines represent unstable equilibria, drawn to complete the two stable branches in the bistable region. All parameters have default values (Table S1). Note that predators do not go extinct in the given temperature range when $R_{max,T19} = 2.5$ and $E_{R_{max}} = 0$.

4.3 Community composition over temperature and $R_{max,T19}$ for the non-selective predator

Fig. S8 illustrates the community composition and type of dynamics as a function of $R_{max,T19}$ and temperature for a predator feeding with equal intensity on both consumer life stages, given different temperature-scaling scenarios. This is the $p = 0.5$-equivalent of Fig. 2 (main text). For the

corresponding biomass densities of the state variables for selected $R_{max,T19}$-values, see Fig. S9. The temperature at which the cyclic dynamics of the food chain switch to fixed point dynamics increases with $R_{\mathrm{max,T19}}$, as does the temperature at which the predator goes extinct. Note also that with equal feeding intensity on both life stages warming does not cause bistability.

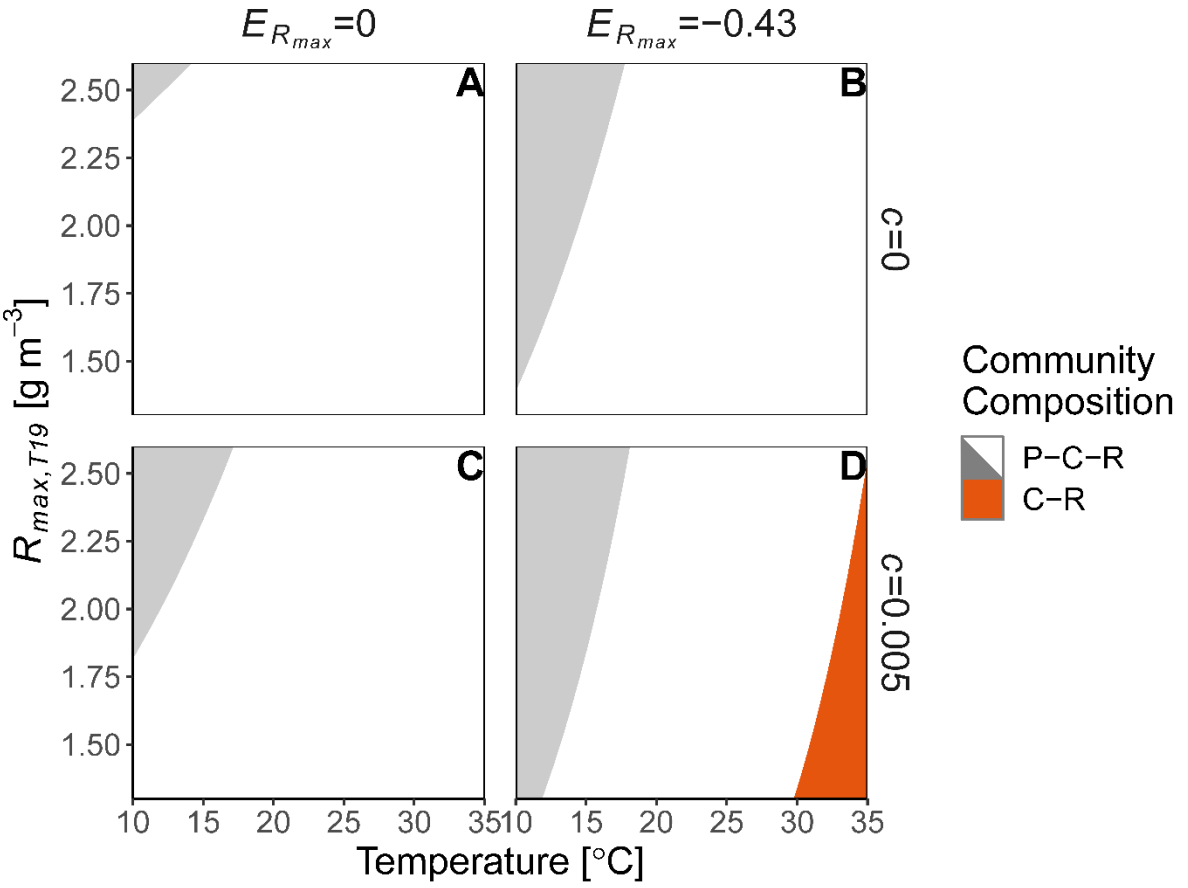

Fig. S8. Effects of temperature on community structure depend on temperature scaling of $R_{max,T19}$ and whether metabolism scales with body size and temperature independently ($c = 0$) or interactively ($c \neq 0$) in the consumer (C) and predator (P). With warming, the tri-trophic food-chain changes from cyclic (grey space), to stable dynamics (white space), to being reduced to two trophic levels following predator extinction (dark orange space). The figure shows how the species composition and dynamics of the food-chain change with temperature and $R_{max,T19}$, given no ($E_{R_{max}} = 0$) (A, C) or negative ($E_{R_{max}} = -0.43$) (B, D) effects of temperature on $R_{max,T19}$, with independent (A, B) or interactive (C, D) effects of body size and temperature on metabolism. The predator feeds on both consumer life stages ($p = 0.5$), all other parameters have default values.

4.4 Equilibrium biomass densities over temperature for different $\boldsymbol{R_{max,T19}}$ ($\boldsymbol{p = 0.5}$)

Fig. S9 illustrates the change in equilibrium biomass densities over temperature for three selected $R_{max,T19}$-values used in Fig. S8, representing high, medium and low $R_{max,T19}$-values. This shows that warming causes the predator biomass density to decline (but note no extinction occurs in the

452 temperature range), and that this decline is more rapid when $R_{max,T19}$ also declines with temperature
453 (Fig. S9 E-H versus Fig. S6 A-D).
454

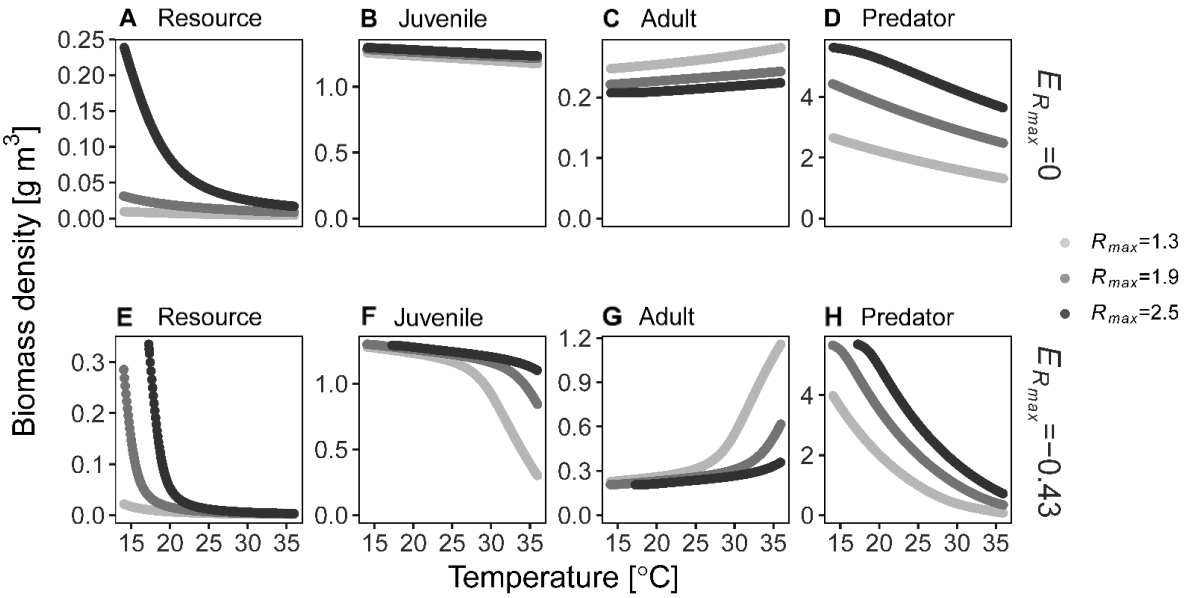

455
456 **Fig. S9.** Equilibrium biomass densities of the resource (A, E), juvenile (B, F) and adult (C, G)
457 consumers and predator (D, H) as a function of temperature for three different levels of $R_{max,T19}$. The
458 chosen $R_{max,T19}$ levels reflect the range of values used in Fig. S8 for the predator feeding with equal
459 intensity on both life stages ($p = 0.5$). The top row shows biomass densities when assuming no effect
460 of temperature on $R_{max,T19}$. In the bottom row it is assumed that $R_{max,T19}$ decreases with temperature
461 ($E_{R_{max}} = 0$ and -0.43, respectively). Only stable equilibria are shown. All parameters have default
462 values.

463 ## 4.5 Community structure shifts with temperature and the predators' feeding preference

464 Fig. S10 shows the location of bifurcations corresponding to changes in stability and stage structure as
465 a function of predators feeding preference (p) and temperature, using the empirical model. This analysis
466 is the empirical model's analogue to Fig. 3A (main text) and illustrates the close resemblance between
467 the two alternative model parameterization in this scenario.

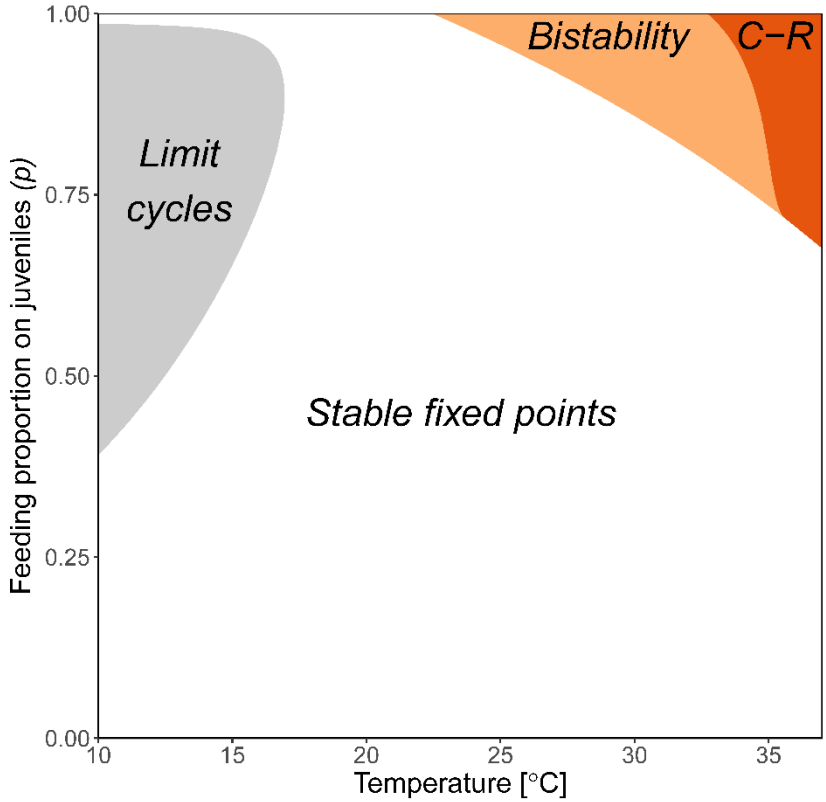

Fig. S10 Community structure shifts with temperature and the predators' feeding preference. In grey regions all species in the food-chain exhibit stable population cycles, white corresponds to stable predator-consumer-resource states, orange shows bistable regions where the food-chain exhibits alternative stable states with predators being either extinct or abundant (here the lower temperature boundary of the region corresponds to the invasion boundary and the upper is the persistence boundary), and dark orange is the stable consumer-resource system where predators cannot persist. $E_{R_{max}} = -0.43$, all other parameters have default values.

4.6 Persistence temperature for different predator feeding preferences and variation in activation energy

The temperature dependence of individual-level rates can be highly variable, especially within species (Dell *et al.* 2011a; Englund *et al.* 2011a). In addition, the relative activation energy of vital rates can also determine the effect of temperature on population dynamics (Vasseur & McCann 2005; O'Connor *et al.* 2011; Fussmann *et al.* 2014; Uszko *et al.* 2017). Therefore, we conducted an additional analysis in which the activation energy of functional response parameters ($a_{J,A,P}$ and $I_{max,J,A,P}$) was scaled by a factor of 0.5 and 1.5 relative to metabolic rate ($E_M = 0.594$). This results in E_I-values between 0.297 and 0.891, which are in the range of estimates reported in the literature (Dell *et al.* 2011b; Englund *et al.* 2011b). This analysis corroborates that a juvenile specialized predator has the lowest persistence (in terms of temperature at extinction), in the empirical model (Fig. 1, main text), followed by a non-

specialized predator and eventually the adult-specialized ($p = 0$), which could persist at the highest temperature (Fig. S11). It also shows that the activation energies of metabolic rate and functional response parameters only regulate at what temperatures bifurcations occur (i.e. predator extinctions, onset of alternative stable states), and not *if* they occur, which instead is determined by feedbacks between food-and size-dependent life history processes in combination with predator feeding preference. This is in contrast to unstructured models, where the effects of warming on stability and persistence largely can be predicted from the temperature dependence of energetic efficiency (Uszko *et al.* 2017). Similar results were also found in (Lindmark *et al.* 2018). However, when feeding rates are more temperature sensitive than metabolism ($E_I > E_M$), extinctions or bistability does not occur in the studied temperature range for a predator feeding only on juveniles (Fig. S11-S12).

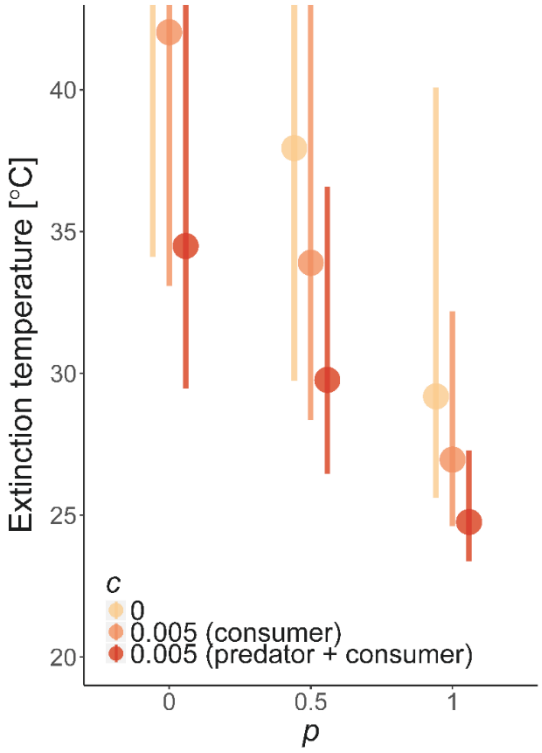

Fig. S11. Predator starvation temperature as a function of predator feeding preference for different interactive effects of size and temperature (c). Yellow points are from simulations with no temperature-size interaction for metabolism ($c = 0$), orange points are from $c = 0.005$ for consumers only and red points show scenarios in which both consumers and predators have interactive temperature-size scaling ($c = 0.005$). Lines correspond to scenarios in which the activation energy of functional response parameters where scaled by 0.5 and 1.5 relative to metabolism activation energy, to mimic scenarios with different feeding efficiencies (size-independent). Note that bistable dynamics are not highlighted in this figure for $p = 1$. $E_{R_{max}} = -0.43$ and $R_{max,T19} = 1.3$ g m^3, all other parameters have default values.

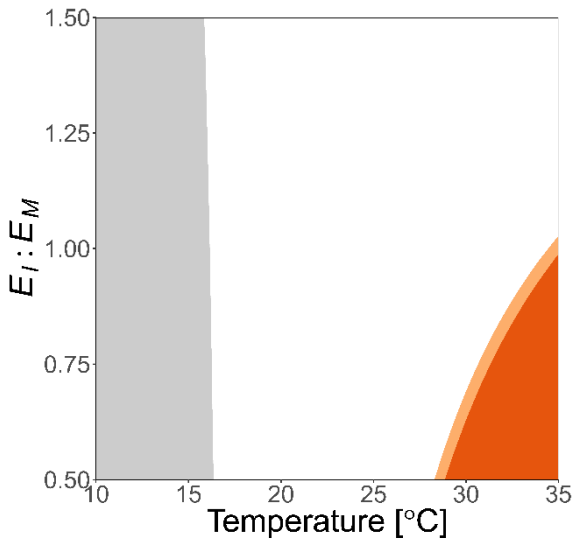

Fig. S12. Community structure shifts with temperature and the activation energy of functional response parameters relative to the activation energy of metabolism ($E_M = 0.594$). In grey regions all species in the food chain exhibit stable population cycles, white corresponds to stable predator-consumer-resource states, orange shows bistable regions where the food chain exhibits alternative stable states with predators being either extinct or absent (here the lower temperature boundary of the region corresponds to the invasion boundary and the upper is the persistence boundary), and dark orange is the stable consumer-resource system where predators cannot persist. $E_{R_{max}} = -0.43$, all other parameters have default values.

4.7 Effects of warming on predator biomass densities under different scenarios of energetic efficiency

When the energetic efficiency is temperature-independent in the consumer and predator, such that there is no change in the relative increase of gains (ingestion) versus losses (metabolism, mortality) with temperature, the activation energy of the basal resource turnover rate (E_δ) does not qualitatively matter for the effect of warming on predator biomass if maximum resource density decreases with the same rate as turnover rate increases ($E_{R_{max}} = -E_\delta$) (see Table S5, in which $E_I = E_M = E_\mu = 0.594$ was assumed). However, with a temperature-independent $R_{max,T19}$ ($E_{R_{max}} = 0$), predator biomass density increases if resource turnover rate increases faster with temperature than consumer and predator feeding, metabolism and mortality, i.e. $E_\delta > E_{I,M,\mu}$. When $R_{max,T19}$ increases with temperature ($E_{R_{max}} = 0.63$), predator biomass density always increases with temperature (Table S5).

Table S5. Predator biomass responses to warming for different cases of temperature dependences in the basal resource. When predator biomass declines, the persistence- and invasion boundaries (limit point and branch point, respectively) are shown. E_δ-values are arbitrarily chosen to fulfil the conditions $E_\delta > E_{I,M,\mu}$, $E_\delta = E_{I,M,\mu}$ and $E_\delta < E_{I,M,\mu}$. $E_{R_{max}}$ is assumed to be -E_δ, E_δ or 0, as in the main analyses and $E_{I,M,\mu} = 0.594$. While arbitrarily chosen, these values are still in the range of

empirical estimates, see section 2 and (Savage et al. *2004). $p = 1$, All other parameters have default values (Table S2). Note, these equilibrium continuations all start from a stable equilibrium, as the temperature scalar equal 1 at reference temperature.*

E_δ	$E_{R_{max}}$	**Predator biomass response to warming (>19 °C)**
0.63	0	*Increasing*
0.63	-0.63	*Decreasing* • Persistence boundary: 33 °C • Invasion boundary: 23.2 °C
0.63	0.63	*Increasing*
0.59	0	*No change*
0.59	-0.59	*Decreasing* • Persistence boundary: 33 °C • Invasion boundary: 23.2 °C
0.59	0.59	*Increasing*
0.55	0	*Decreasing* • Persistence boundary: > 36 °C • Invasion boundary: > 36 °C
0.55	-0.55	*Decreasing* • Persistence boundary: 33 °C • Invasion boundary: 23.2 °C
0.55	0.55	*Increasing*

Table S5 shows that predator biomass only increases with warming when $E_\delta > E_{I,M,\mu}$, given that $R_{max,T19}$ is temperature-independent and $E_I = E_M = E_\mu = 0.594$, or when R_{max} increases with temperature. In Table S6, we assess the effect of temperature on predator biomass density for the scenario $E_\delta > E_M$, while also varying the effect of temperature on the energetic efficiency of consumers and predators. This shows that predator biomass density can decline with increasing temperatures even when $E_\delta > E_{I,M,\mu}$ and $R_{max,T19}$ is temperature-independent, given that predator and consumer energetic efficiency declines with temperature. As in Table S5, predator biomass density increases when R_{max} increases with temperature. If also the energetic efficiency declines with temperature, warming eventually induces limit cycles (Hopf bifurcation at *28.4* °C*).*

Table S6. Predator biomass responses to warming for different cases of temperature dependences in the basal resource using the empirical model. When predator biomass declines, the persistence- and invasion boundaries (limit point and branch point, respectively) are shown. The temperature dependence of feeding rates are varied relative to the activation energy of metabolism and mortality, the two loss terms for biomass ($E_M = E_\mu = 0.594$) to capture different effects of temperature on

549 *the energetic efficiency of consumers and predators, given* $E_\delta = 0.63$, $E_{R_{max}} = 0, -0.63$ *or 0.63 and* $p = 1$. *All other*
550 *parameters have default values (Table S2).*

E_I: $E_{M,\mu}$	E_δ	$E_{R_{max}}$	**Predator biomass response to warming (>19 °C)**
1.5	0.63	0	*Increasing*
1.5	0.63	-0.63	*Decreasing* • Persistence boundary: > 36 °C • Invasion boundary: 26.9 °C
1.5	0.63	0.63	*Increasing*
1	0.63	0	*Increasing*
1	0.63	-0.63	*Decreasing* • Persistence boundary: 33 °C • Invasion boundary: 23.2 °C
1	0.63	0.63	*Increasing*
0.5	0.63	0	*Decreasing* • Persistence boundary: > 36 °C • Invasion boundary: 29.6 °C
0.5	0.63	-0.63	*Decreasing* • Persistence boundary: 27.9 °C • Invasion boundary: 21.8 °C
0.5	0.63	0.63	*Increasing until onset of limit cycles (Hopf bifurcation at 28.4* °C)

551 ## 4.8 Mean body size of the community under warming

552 We also calculated biomass-weighted mean body size (S_T) of the community for stable equilibria at
553 temperature T (averaged for each T) as $S_T = \frac{\sum_s (S_s \cdot B_{s,T})}{\sum_s B_{s,T}}$, where S_s is the representative body size of
554 juvenile consumers, adult consumers or predators ($s = J, A, P$) and $B_{s,T}$ is their corresponding
555 equilibrium biomass density at temperature T. The general decline in predator biomass with increased
556 temperatures leads to a decline in the biomass-weighted mean community body size (Fig. S13). As with
557 the abrupt predator collapse, the community size structure can also show a non-gradual abrupt decline
558 as temperature increases, leading to alternative stable "community size states".

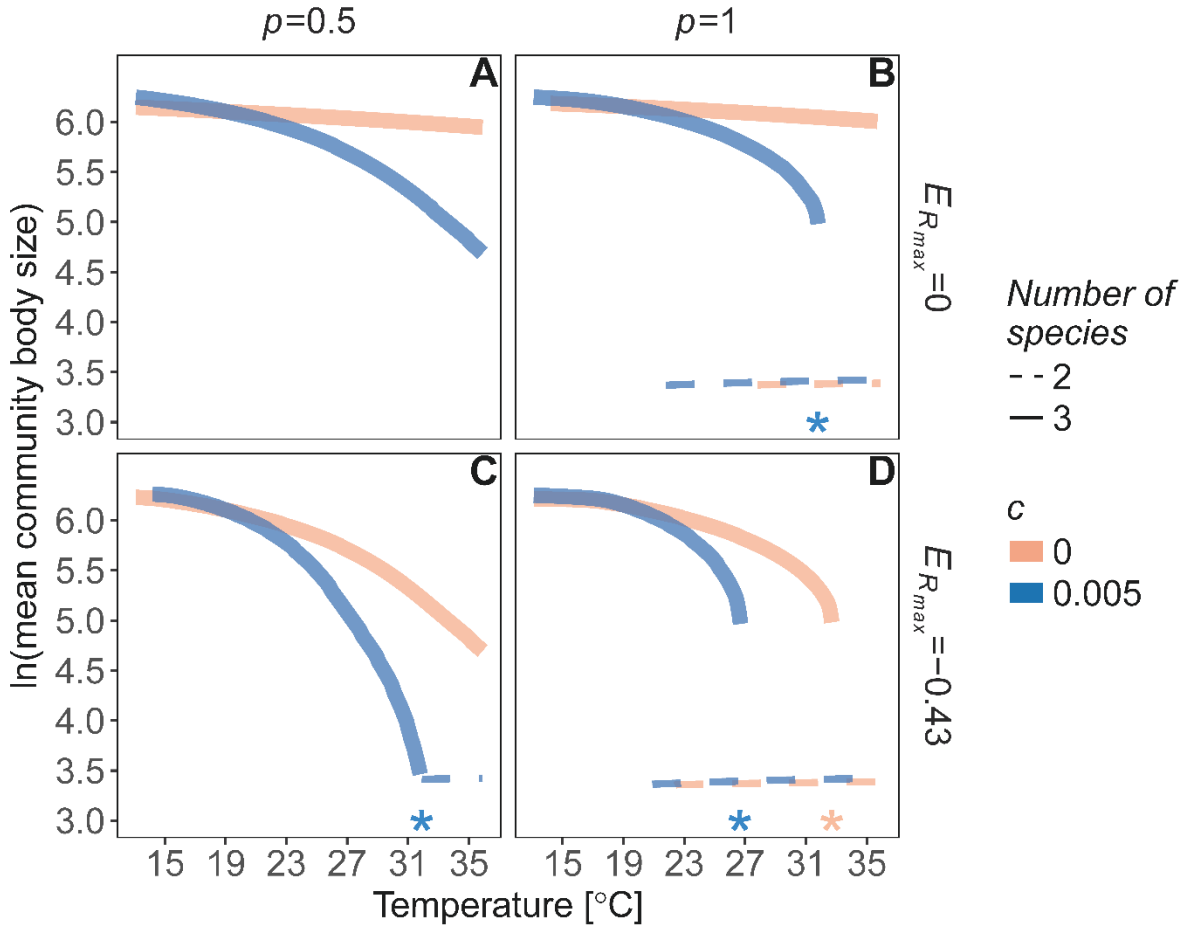

559

560 **Fig. S13** Mean body size (S_T) in the community decreases with temperature, and warming can induce
561 abrupt shifts in mean community body size. The warming effects on S_T depend on maximum resource
562 density ($R_{max,T19}$), ecological interactions and temperature-size interactions, as shown for food-chains
563 with a predator species feeding with equal intensity on both consumer life stages (A, C) ($p = 0.5$) or
564 exclusively on juveniles (B, D) ($p = 1$), in a system with no temperature effects (A, B) on $R_{max,T19}$
565 ($E_{R_{max}} = 0$) or declining $R_{max,T19}$ with temperature (C, D) ($E_{R_{max}} = -0.43$). Colors indicate different
566 temperature-size scaling of metabolism, where coral lines show independent effects of body size and
567 temperature, $c = 0$ and blue lines show positive interactive effects, $c = 0.005$. Dashed curves
568 correspond to equilibria in which the predator has gone extinct, and mean community body size
569 correspondingly has shifted to smaller values. Stars indicate the maximum temperature for predator
570 persistence. Parameters have default values.

571 5. Generic stage-structured biomass model

572 In order to explore the robustness and generality of our results, we also analysed selected temperature-
573 scaling scenarios in a simpler model with respect to model functions and assumptions. This model (Box
574 4.1 and 4.2 in (De Roos & Persson 2013)) is a tri-trophic and temperature-dependent version of the

original (generic) stage-structured biomass model (De Roos *et al.* 2007, 2008), to which we add temperature dependence in the same way as the empirical model (see main text). All dynamical equations are the same as presented in Eqns. 1-4 in the main text. The model is described in Table S7-S8 (note some variable names may be overlapping with the empirical model because we wanted to keep the same variable names as in the original formulation) (De Roos & Persson 2013).

The main motivation for using the generic model for comparison lies in its simplicity. Specifically, in the generic model (De Roos *et al.* 2008), it is assumed that individual-level and mass-specific rates (intake, maintenance, mortality) scale linearly with body size. Life stage specific competitive ability (leading to ontogenetic asymmetry if not identical) is implemented by scaling the resource intake by adults in relation to resource intake by juveniles with a single parameter q (Table S7). This asymmetry in turn determines which life stage exhibits biomass overcompensation in response to mortality, and thus whether emergent Allee effects and bistability occurs with warming. This is a more phenomenological implementation of ontogenetic asymmetry compared to our empirical model, where asymmetry emerges because vital rates scale sub-linearly with body size and consumer life stages are characterized by different body sizes. For example, in the empirical model, feeding rates and metabolism stem from single species experiments or data and thus are more realistic. The parameters in the generic model stem from averages from inter-specific relationships (e.g. ectotherm invertebrates) (De Roos & Persson 2013). However, while the generic parameterization is more phenomenological, it can be used to generalize the results of the empirical model and show how they emerge because of the specific type of asymmetry in the empirical model (i.e. juveniles being competitively superior to adults). Another important difference is that the generic parameterization uses a Monod-equation (Monod 1949) with a size independent (constant) half saturation resource density, as opposed to the Holling Type II functional response with a size-dependent attack rate in our default, empirical parameterization.

We implement temperature dependence in the generic model in the same way as in the empirical model, i.e. by scaling the parameters resource turnover (ρ), maximum resource density (R_{max}), maximum intake rate ($M_{C,P}$), background mortality ($\mu_{C,P}$) and maintenance ($T_{C,P}$) with the Boltzmann-Arrhenius function $e^{\frac{E_Y(T-T_0)}{kTT_0}}$, where E_Y refers to the activation energy of the corresponding rate (same as in the empirical model, see Table S2 for values).

Table S7 Model equations and functions of the original (generic) stage-structured biomass model

Dynamic equations	**Description**
$\boldsymbol{\frac{dR}{dt} = G(R) - \omega_J(R)J - \omega_A(R)A}$	Resource biomass dynamics
$\boldsymbol{\frac{dJ}{dt} = v_A^+(R)A - \gamma\left(v_J^+, d_J\right)J + v_J(R)J - d_J(P)J}$	Biomass dynamics of juveniles
$\boldsymbol{\frac{dA}{dt} = \gamma\left(v_J^+, d_J\right)J + (v_A(R) - v_A^+(R))A - d_A(P)A}$	Biomass dynamics of adults

$\frac{dP}{dt} = (v_P(J,A) - \mu_P)P$		Biomass dynamics of predators
Function	**Expression**	**Description**
$G(R,T)$	$\rho(R_{max} - R)$	Intrinsic resource turnover
$\omega_J(R)$	$M_c R/(H_c + R)$	Resource intake by juveniles
$\omega_A(R)$	$qM_c R/(H_c + R)$	Resource intake by adults
$v_J(R)$	$\sigma_c \omega_J(R) - T_c$	Net energy production of juveniles
$v_A(R)$	$\sigma_c \omega_A(R) - T_c$	Net energy production of adults
$d_J(P)$	$\mu_J + \frac{M_P \phi P}{H_p + \phi J + (1-\phi)A}$	Mortality rate of juveniles
$d_A(P)$	$\mu_A + \frac{M_P (1-\phi) P}{H_p + \phi J + (1-\phi)A}$	Mortality rate of adults
$\gamma(v_J^+, d_J)$	$(v_J^+(R) - d_J(P))/(1 - z^{(1-\frac{d_J(P)}{v_J^+(R)})})$	Maturation rate of juveniles
$v_P(J,A)$	$\sigma_P M_P \frac{\phi J + (1-\phi)A}{H_p + \phi J + (1-\phi)A} - T_P$	Net energy production of predators

Table S8 Parameters in the original (generic) stage-structured biomass model. See Box. 3.4 in De Roos & Persson (2013).

Parameter	Value	Unit	Description
Resource			
ρ	0.1	day^{-1}	Resource turnover rate
R_{max}	18	mg/L	Resource maximum biomass density
Prey			
W_A	0.0001	g	
M_c	$0.1 W_A^{-0.25}$	day^{-1}	Mass-specific maximum ingestion rate
H_c	3	mg/L	Ingestion half-saturation resource density
q	0.5 or 2	-	Adult-juvenile consumer ingestion ratio
T_c	$0.01 W_A^{-0.25}$	day^{-1}	Mass-specific maintenance rate
σ_c	0.5	-	Conversion efficiency
z	0.01 when $q = 0.5$; 0.5 when $q = 2$	-	New born-adult consumer size ratio
μ_J	$0.0015 W_A^{-0.25}$	day^{-1}	Juvenile background mortality rate

$\boldsymbol{\mu_A}$	$0.0015W_A^{-0.25}$	day^{-1}	Adult background mortality rate
Predator			
$\boldsymbol{W_P}$	0.01	g	
$\boldsymbol{M_P}$	$0.1W_P^{-0.25}$	day^{-1}	Mass-specific maximum ingestion rate
$\boldsymbol{H_P}$	3	mg/L	Ingestion half-saturation resource density
$\boldsymbol{T_P}$	$0.01W_P^{-0.25}$	day^{-1}	Mass-specific maintenance rate
$\boldsymbol{\sigma_P}$	0.5	-	Conversion efficiency
$\boldsymbol{\mu_P}$	$0.0015W_P^{-0.25}$	day^{-1}	Predator background mortality rate
$\boldsymbol{\phi}$	0.0-1.0	-	Predator foraging preference for juveniles

6. Assessing the sensitivity to model functions using a generic model

In addition to evaluating parameter sensitivity of model results we also assessed the sensitivity of the model with respect to model functions, using the generic model parameterization (De Roos *et al.* 2007; De Roos & Persson 2013). This also allowed us to test the correspondence between the empirical model with its more complex empirically derived parameterization and the simpler, more phenomenological generic parameterization, and to generalize the results by showing that the type of regulation in the consumer population determines the effect of stage-specific predation on stability and persistence (see Fig. 3, main text). Fig. S14 shows the equilibrium biomass densities over temperature using the generic model parameterization coupled with the default temperature scaling. Qualitatively the results are very similar to those shown in Fig. 1 (main text), which are based on the analogues analysis using the empirical model.

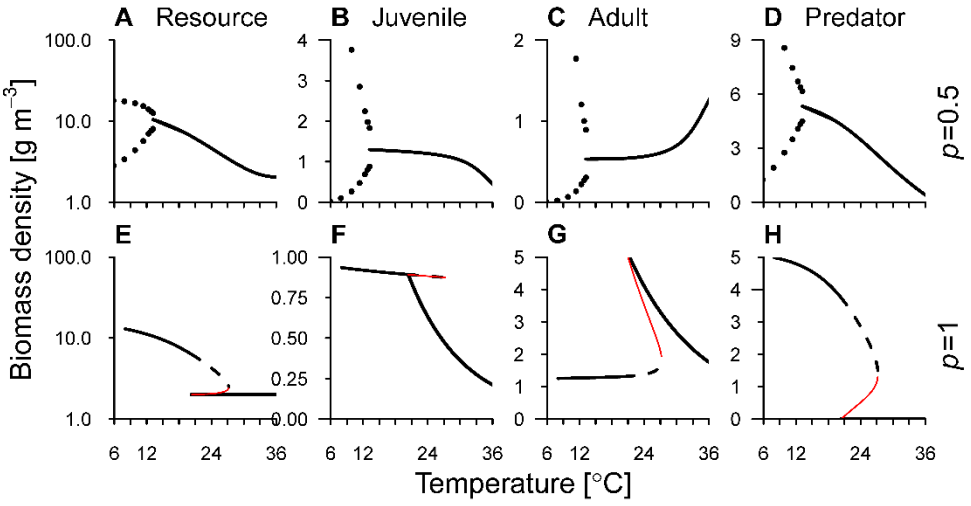

Fig. S14. Effects of warming on food chain stability depend on ecological interactions – generic model parameterization (De Roos *et al.*, 2007) with added temperature-dependence. Equilibrium biomass

densities of the resource (A, E), consumer life stages (B-C, F-G) and predator (D, H) as a function of temperature, given a predator feeding with equal intensity on both life stages (A-D) ($\boldsymbol{\phi} = 0.5$) or exclusively on juveniles (E-H) ($\boldsymbol{\phi} = 1$). Black lines (solid and dashed) are stable equilibria and red thin lines are unstable equilibria (connecting the two stable branches in the bistable region), which separate the two stable equilibria when there are alternative stable states. Maximum and minimum biomass density of a stable limit cycle is shown with points (top row below ~13 °C). Alternative stable states, where predators are either extinct or abundant, occur between ~21-30 °C in E-H. Note the different scales on the y-axes and the logarithmic y-axis for resources densities. $E_{R_{max}} = -0.43$, $q = 0.5$, all other parameters have default values (SI Appendix S2, Table S8).

Cited literature

Armstrong, J.D. & Hawkins, L.A. (2008). Standard metabolic rate of pike, Esox lucius: variation among studies and implications for energy flow modelling. *Hydrobiologia*, 601, 83–90.

Armstrong, J.D., Priede, I.G. & Lucas, M.C. (1992). The link between respiratory capacity and changing metabolic demands during growth of northern pike, Esox lucius L. *Journal of Fish Biology*, 41, 65–75.

Byström, P. & Andersson, J. (2005). Size-dependent foraging capacities and intercohort competition in an ontogenetic omnivore (Arctic char). *Oikos*, 110, 523–536.

Byström, P. & García-Berthou. (1999). Density dependent growth and size specific competitive interactions in young fish. *Oikos*, 86, 217–232.

Claessen, D., De Roos, A.M. & Persson, L. (2000). Dwarfs and Giants: Cannibalism and Competition in Size-Structured Populations. *The American Naturalist*, 155, 219–237.

De Roos, A.M. & Persson, L. (2001). Physiologically structured models - from versatile technique to ecological theory. *Oikos*, 94, 51–71.

De Roos, A.M. & Persson, L. (2013). *Population and community ecology of ontogenetic development*. Princeton University Press.

De Roos, A.M., Schellekens, T., van Kooten, T., van De Wolfshaar, K.E., Claessen, D. & Persson, L. (2008). Simplifying a physiologically structured population model to a stage-structured biomass model. *Theoretical Population Biology*, 73, 47–62.

De Roos, A.M., Schellekens, T., van Kooten, T., van de Wolfshaar, K.E., Claessen, D. & Persson, L. (2007). Food-dependent growth leads to overcompensation in stage-specific biomass when mortality increases: the influence of maturation versus reproduction regulation. *The American Naturalist*, 170, E59–E76.

Dell, A.I., Pawar, S. & Savage, V.M. (2011a). Systematic variation in the temperature dependence of physiological and ecological traits. *Proceedings of the National Academy of Sciences, USA*, 108, 10591–10596.

Dell, A.I., Pawar, S. & Savage, V.M. (2011b). Systematic variation in the temperature dependence of physiological and ecological traits. *Proceedings of the National Academy of Sciences, USA*, 108, 10591–10596.

van Denderen, P.D. & van Kooten, T. (2013). Size-based species interactions shape herring and cod population dynamics in the face of exploitation. *Ecosphere*, 4, 1–15.

Diana, J.S. (1982). An experimental analysis of the metabolic rate and food utilization of northern pike. *Comparative Biochemistry and Physiology – Part A: Physiology*, 71, 395–399.

Downs, C.J., Hayes, J.P. & Tracy, C.R. (2008). Scaling metabolic rate with body mass and inverse body temperature: A test of the Arrhenius fractal supply model. *Functional Ecology*, 22, 239–244.

Englund, G., Öhlund, G., Hein, C.L. & Diehl, S. (2011a). Temperature dependence of the functional response. *Ecology Letters*, 14, 914–921.

Englund, G., Öhlund, G., Hein, C.L. & Diehl, S. (2011b). Temperature dependence of the functional response. *Ecology Letters*, 14, 914–921.

Froese, R., Thorson, J.T. & Reyes, R.B. (2014). A Bayesian approach for estimating length-weight relationships in fishes. *Journal of Applied Ichthyology*, 30, 78–85.

Fussmann, K.E., Schwarzmüller, F., Brose, U., Jousset, A. & Rall, B.C. (2014). Ecological stability in response to warming. *Nature Climate Change*, 4, 206–210.

Gilbert, B., Tunney, T.D., McCann, K.S., DeLong, J.P., Vasseur, D.A., Savage, V.M., *et al.* (2014). A bioenergetic framework for the temperature dependence of trophic interactions. *Ecology Letters*, 17, 902–914.

Gillooly, J.F., Brown, J.H., West, G.B., Savage, V.M. & Charnov, E.L. (2001). Effects of size and temperature on metabolic rate. *Science*, 2248–2251.

Groot, C. (2010). *Physiological Ecology of Pacific Salmon*. UBC Press.

Heikinheimo, O. & Korhonen, A.P. (1996). Food consumption of northern pike (Esox lucius L .), estimated with a bioenergetics model. *Ecology of Freshwater Fish*, 5, 37–47.

Hjelm, J. & Persson, L. (2001). Size-dependent attack rate and handling capacity: inter-cohort competition in a zooplanktivorous fish. *Oikos*, 95, 520–532.

Hölker, F. (2000). Bioenergetik dominanter Fischarten (Abramis brama (Linnaeus, 1758) und Rutilus rutilus (Linnaeus, 1758)) in einem eutrophen See Schleswig-Holsteins: Ökophysiologie und individuen-basierte Modellierung. PhD Thesis. Verein zur Förderung der Ökosystemforschung zu Kiel.

Hölker, F. & Haertel, S.S. (2004). Application of a bioenergetics model to roach. *Journal of Applied Ichthyology*, 20.

Holling, C.S. (1959). Some characteristics of simple types of predation and parasitism. *Canadian Entomologist*, 91, 385–398.

692 Karås, P. & Thoresson, G. (1992). An application of a bioenergetics model to Eurasian perch (Perca
693 fluviatilis L.). *Journal of Fish Biology*, 41, 217–230.

694 van Leeuwen, A., De Roos, A.M. & Persson, L. (2008). How cod shapes its world. *Journal of Sea*
695 *Research*, 60, 89–104.

696 Lindmark, M., Huss, M., Ohlberger, J. & Gårdmark, A. (2018). Temperature-dependent body size
697 effects determine population responses to climate warming. *Ecology Letters*, 21, 181–189.

698 Lumb, C.E., Johnson, T.B., Cook, H.A. & Hoyle, J.A. (2007). Comparison of lake whitefish
699 (Coregonus clupeaformis) growth, condition, and energy density between Lakes Erie and
700 Ontario. *Journal of Great Lakes Research*, 33, 314–325.

701 Mitchell, S.E., Halves, J. & Lampert, W. (2004). Coexistence of similar genotypes of Daphnia magna
702 in intermittent populations: response to thermal stress. *Oikos*, 106, 469–478.

703 Monod, J. (1949). The growth of bacterial cultures. *Annu. Rev. Microbiol.*, 3, 371–394.

704 O'Connor, M.I., Gilbert, B. & Brown, C.J. (2011). Theoretical predictions for how temperature
705 affects the dynamics of interacting herbivores and plants. *The American Naturalist*, 178, 626–
706 638.

707 Ohlberger, J., Edeline, E., Vollestad, L.A., Stenseth, N.C. & Claessen, D. (2011). Temperature-driven
708 regime shifts in the dynamics of size-structured populations. *The American Naturalist*, 177,
709 211–223.

710 Ohlberger, J., Mehner, T., Staaks, G. & Hölker, F. (2012). Intraspecific temperature dependence of
711 the scaling of metabolic rate with body mass in fishes and its ecological implications. *Oikos*,
712 121, 245–251.

713 Persson, L., Amundsen, P.-A., M., D.R.A., Klemetsen, A., Knudsen, R. & Primicerio, R. (2007).
714 Culling prey promotes predator recovery - alternative states in a whole-lake experiment.
715 *Science*, 316, 1743–1746.

716 Persson, L., Bertolo, A. & De Roos, A.M. (2006). Temporal stability in size distributions and growth
717 rates of three Esox lucius L. populations. A result of cannibalism? *Journal of Fish Biology*,
718 69, 461–472.

719 Persson, L. & De Roos, A.M. (2013). Symmetry breaking in ecological systems through different
720 energy efficiencies of juveniles and adults. *Ecology*, 94, 1487–1498.

721 Persson, L., Leonardsson, K., De Roos, A.M., Gyllenberg, M. & Christensen, B. (1998). Ontogenetic
722 scaling of foraging rates and the dynamics of a size-structured consumer-resource model.
723 *Theoretical Population Biology*, 54, 270–293.

724 Peters, R.H. (1983). *The ecological implications of body size*. Cambridge University Press.

725 Pothoven, S.A., Nalepa, T.F., Madenjian, C.P., Rediske, R.R., Schneeberger, P.J. & He, J.X. (2006).
726 Energy density of lake whitefish Coregonus clupeaformis in Lakes Huron and Michigan.
727 *Environmental Biology of Fishes*, 76, 151–158.

R Core Team. (2018). *R: A Language and Environment for Statistical Computing. R Foundation for Statistical Computing*. Vienna, Austria.

Savage, V.M., Gillooly, J.F., Brown, J.H., West, G.B. & Charnov, E.L. (2004). Effects of body size and temperature on population growth. *The American Naturalist*, 163, 429–441.

Stoessel, D.J. (2014). Age, growth, condition and reproduction of roach Rutilus rutilus (Teleostei: Cyprinidae), in south-eastern Australia. *Marine & Freshwater Research*, 65, 275–281.

Uszko, W., Diehl, S., Englund, G. & Amarasekare, P. (2017). Effects of warming on predator-prey interactions: a resource-based approach and a theoretical synthesis. *Ecology Letters*, 20, 513–523.

Vasseur, D.A. & McCann, K.S. (2005). A mechanistic approach for modelling temperature-dependent consumer-resource dynamics. *The American Naturalist*, 166, 184–198.

van de Wolfshaar, K.E., De Roos, A.M. & Persson, L. (2006). Size-Dependent Interactions Inhibit Coexistence in Intraguild Predation Systems with Life-History Omnivory. *American Naturalist*, 168, 62–75.

van de Wolfshaar, K.E., Schellekens, T., Poos, J.J. & van Kooten, T. (2012). Interspecific Resource Competition Effects on Fisheries Revenue. *PLoS ONE*, 7.